Carbohydrate Polymers 90 (2012) 957–966

Contents lists available at SciVerse ScienceDirect

Carbohydrate Polymers

journal homepage: www.elsevier.com/locate/carbpol

LBL fabricated biopolymer-layered silicate based nanofibrous mats and their cell compatibility studies

Rong Huang[a,1], Yuejun Li[b,1], Xue Zhou[c], Qi Zhang[a], Huanguang Jin[a], Jiemin Zhao[a], Siyi Pan[a], Hongbing Deng[a,*]

[a] College of Food Science and Technology and the MOE Key Laboratory of Environment Correlative Dietology, Huazhong Agricultural University, No. 1 Shizishan Road, Wuhan 430070, China

[b] Department of Plastic Surgery, Tangdu Hospital, Fourth Military Medical University, Xi'an, 710038, China

[c] Department of Occupational and Environmental Health and the MOE Key Laboratory of Environment and Health, School of Public Health, Tongji Medical College, Huazhong University of Science and Technology, Wuhan 430030, China

ARTICLE INFO

Article history:
Received 14 May 2012
Received in revised form 7 June 2012
Accepted 11 June 2012
Available online 18 June 2012

Keywords:
Organic rectorite
Nanofibrous mats
Layer-by-layer
Cell compatibility

ABSTRACT

N-(2-hydroxyl) propyl-3-trimethyl ammonium chitosan chloride (HTCC) was synthesized from chitosan (CS). Organic rectorite (OREC) added into cellulose acetate (CA) was used to fabricate electrospun nanofibrous mats with improved thermal properties, as a result of depositing multilayers of the positively charged HTCC-OREC composites and the negatively charged sodium alginate (ALG) via layer-by-layer (LBL) technique. The morphology was affected by the number of deposition bilayers and the component of the outmost layer. Observed from the field emission scanning electron microscopy (FE-SEM) images, the LBL structured nanofibrous mats had much larger fiber sizes than CA-OREC nanofibrous mats. X-ray photoelectron spectroscopy (XPS) and X-ray diffraction (XRD) results further confirmed that HTCC-OREC was assembled on nanofibrous mats. Additionally, cell experiments and MTT results demonstrated that OREC had little effect on the cytotoxicity of LBL template, but obviously affected both the cytotoxicity and the cell compatibility of LBL structured mats when OREC was in the deposition films.

1. Introduction

In the past decades, the development of polymer/layered silicate nanofibers has drawn much attention because it could combine the unique physical and chemical properties of both inorganic and organic materials. The composites also possess characteristics of nanofibers such as ultrafine diameter, high surface area-to-volume ratio, three dimensional (3D) nanofibrous structure, etc. (Deng et al., 2010; Deng, Li, et al., 2011). Recently, many researchers have focused on this kind of composite nanofibers for a number of applications, including drug delivery, bacterial inhibition and food packaging. Polymer/layered silicate does exhibit improved properties compared to the polymer itself, especially thermal and mechanical properties (Wang et al., 2006, 2009; Xu et al., 2012). However, less attention so far been drawn to the cell compatibility of polymers/layered silicate composite nanofibers. The safety of the composites must be firstly taken into consideration before any further product design. At this point, it is necessary to explore the compatibility of polymer/layered silicate composite nanofibrous mats to determine the applicability especially in the field of food packaging and biomedicine.

Organic rectorite (OREC), modified from REC, which is a kind of layered silicate, exhibits larger interlayer distance (Deng et al., 2010; Deng, Wang, et al., 2011), better separable layer thickness and larger aspect ratio than montmorillonite (MMT) (Wang et al., 2010). Besides, the European Food Safety Authority (EFSA) reported that bentonite (dioctahedral montmorillonite), another kind of layered silicate, was safe as a food additive (EFSA, 2011). Polymer-layered silicate (PLS) nanocomposites exhibit markedly improved properties when compared with the pure polymers or conventional composites. These include increased modulus and strength, decreased gas permeability, thermal stability and flammability resistance because of their nanometer-size dispersion (Giannelis, 1998; Gilman, 1999; Sinha Ray & Bousmina, 2005). Therefore, layered silicate could be expected to be an ideal candidate in food packing and biomedical applications in future. In our previous reports, it was interesting to note that with the addition of OREC, the bacterial inhibition ability of other antibacterial agents could be remarkably enhanced (Deng, Wang, et al., 2011).

For the fabrication of nanofibers, various methods including electrospinning, phase separation, and template synthesis have been used and electrospinning is considered as an efficient

* Corresponding author. Tel.: +86 27 87282111; fax: +86 27 87282111.
E-mail address: alphabeita3000@yahoo.com.cn (H. Deng).

[1] These authors contributed equally to this work.

0144-8617/$ – see front matter © 2012 Elsevier Ltd. All rights reserved.
http://dx.doi.org/10.1016/j.carbpol.2012.06.026

and simple method because it is straightforward, versatile, cost-effective and scalable (Hartgerink, Beniash, & Stupp, 2001; Reneker & Chun, 1996; Zhang, Venugopal, Huang, Lim, & Ramakrishna, 2005). A wide variety of polymers can be electrospun into fibers and their fiber morphology can be easily controlled by various parameters such as polymer molecular weight, polymer concentration, electrical field applied, and solution feed rate (Boudriot, Dersch, Greiner, & Wendorff, 2006). Electrospun nanofibrous mats have been extensively applied in various areas such as wound dressing, tissue engineering scaffolds, biochemical sensors and cosmetic skin masks (Du & Hsieh, 2009; Huang, Zhang, Kotaki, & Ramakrishna, 2003; Kanani & Bahrami, 2010; Venugopal, Low, Choon, & Ramakrishna, 2008). To further improve the properties of nanofibers in these above applications, the functionalization of nanofibers has become more and more important. Functionalization by the electrostatic layer-by-layer (LBL) self-assembly technique introduced by Decher has become one of the most frequently utilized processes for preparing functional ultra-thin films (Decher, 1997). The LBL self-assembly technique includes step-wise and alternating adsorption of oppositely charged polyelectrolytes, particles (Xiao et al., 2009), and ions on solid templates with different shapes and sizes (Elbakry et al., 2009).

In this study, negatively charged CA-OREC composite nanofibrous mats with good water insolubility were used as an ideal template for LBL deposition for the first time. Positively charged N-(2-hydroxyl) propyl-3-trimethyl ammonium chitosan chloride (HTCC) synthesized from chitosan (CS) was selected as one of the LBL deposition materials. It has been proved that HTCC carries a higher positive charge density and has better bacteria inhibition properties than CS (Qin et al., 2004). Besides, HTCC-OREC composites based nanofibrous mats were found with good antibacterial activity in our previous report (Deng et al., 2012).

The current research focused on generating novel LBL films on nanofibrous polysaccharide-OREC composite template. HTCC-OREC composites and sodium alginate (ALG, a kind of anionic polysaccharide) were selected as deposition materials to be coated on CA-OREC nanofibers via electrostatic LBL self-assembly technique by alternative adsorption of positively charged HTCC-OREC composite and negatively charged ALG in aqueous media. The effects of the number of deposition bilayers, the composition of the multilayer and the component of outermost layer on the formation of the LBL structured nanofibrous mats were investigated. Meanwhile, the cell culture and MTT assay experiments were performed to determine the cell attachment ability and compatibility of the resultant samples.

2. Experimental

2.1. Materials

Cellulose acetate (CA, $M_n = 3 \times 10^4$) was provided by Sigma Aldrich Co., USA. Chitosan (CS, $M_w = 2.1 \times 10^5$ kDa, DD 92%) was purchased from Yuhuan Ocean Biochemical Co. (Taizhou, China). Sodium alginate (ALG, $M_w = 2.5 \times 10^5$ kDa) was supplied by Aladdin Chemical Reagent Co., China. Calcium rectorite (Ca^{2+}-REC) was obtained from Hubei Mingliu Inc. Co. (Wuhan, China). All other chemicals were of analytical grade and used as received. All aqueous solutions were prepared using purified water with a resistance of 18.2 MΩ cm.

N-(2-hydroxyl) propyl-3-trimethyl ammonium chitosan chloride (HTCC), organic rectorite (OREC) and HTCC-OREC composites with the mass ratio of 12/1 were synthesized as described previously (Deng, Li, et al., 2011). CA-OREC nanofibrous mats with the mass ratio of CA:OREC = 10:1 which was fabricated via electrospinning technique was also prepared as reported previously. All as-spun samples were put in vacuum at 60 °C for at least 24 h to remove the trace solvents (Deng, Wang, et al., 2011).

2.2. Formation of LBL structured multilayers on nanofibrous mats

The intercalation solutions for LBL process including HTCC solutions, HTCC-OREC mixed solutions and ALG solutions were prepared with the same concentration of 1 mg/mL by adding them into distilled water with gentle magnetic stirring for 4 h at room temperature, respectively. The pH values of positively charged HTCC and HTCC-OREC solutions were adjusted at 5 and negatively charged ALG was at 4. The ionic strength of all dipping solutions was regulated by the addition of NaCl at a concentration of 0.1 M.

The method for fabricating LBL structured films on nanofibers was identical with our former reports (Deng et al., 2010). First, nanofibrous CA-OREC mats were immersed into HTCC or HTCC-OREC suspensions for 20 min followed by 2 min of rinsing in three pure water baths. The mats were then immersed into the ALG solution for 20 min, followed by the identical rinsing steps. The adsorption and rinsing steps were repeated until the desired number of deposition bilayers was obtained. Here, $(HTCC\text{-}OREC/ALG)_n$ was used as a formula to label the LBL structured films, where n was the number of the HTCC-OREC/ALG bilayers. The outermost layer was HTCC-OREC composite when n equaled to 5.5 and 10.5. The LBL films coated fibrous mats were dried at 60 °C for 24 h under vacuum prior to further characterizations.

2.3. Characterization

The morphology and composition of as-prepared nanofibrous mats were analyzed using field emission scanning electron microscopy (FE-SEM) and energy-dispersive X-ray (EDX) spectroscopy (Sirion 200, FEI, Holland). The samples were sputter coated with gold prior to SEM analysis. The diameters of the fibers were measured using an image analyzer (Adobe Photoshop 7.0). The X-ray diffraction (XRD) was evaluated using diffractometer type D/max-Ra (Rigaku Co., Japan) with Cu target and Ka radiation ($\lambda = 0.154$ nm). The ζ-potential analysis was measured using Nano-25 zetasizer (Malven, England). The thermal stability of prepared mats was determined by differential scanning calorimetry (DSC 204 F1, Zetzsch, Germany) which were heated up twice from 20 to 450 °C with a heating rate of 10 °C/min under nitrogen flow (20 mL/min) to remove the heat history and thermo-gravimetric analysis (TGA, Pyris 1 TGA, PerKinElmer, USA) with a temperature range of 20–500 °C. In order to identify the surface elemental composition, a qualitative analysis was performed with X-ray photoelectron spectroscopy (XPS) using an axis ultra DLD apparatus (Kratos, U.K.).

2.4. Cell adhesion and spreading assay

L929 cells were selected for investigation of the cell compatibility of resultant mats. The prepared scaffolds were cut into round-shaped membrane with a diameter of 6 mm that could fit in sterile tissue culture dishes, then mounted on cover glass and sterilized by UV light for 30 min, washed several times with phosphate buffered saline (PBS) solution prior to cell seeding which facilitated protein absorption and cell attachment onto the nanofibers, then transferred to the 96-well culture plates, L929 cells with a fixed concentration of 1×10^3 per well in 200 μL Dulbecco's Modified Eagle Medium (DMEM) supplemented with 10% fetal bovine serum (FBS) and antibiotics were seeded on all the samples and incubated overnight at 37 °C in humidified

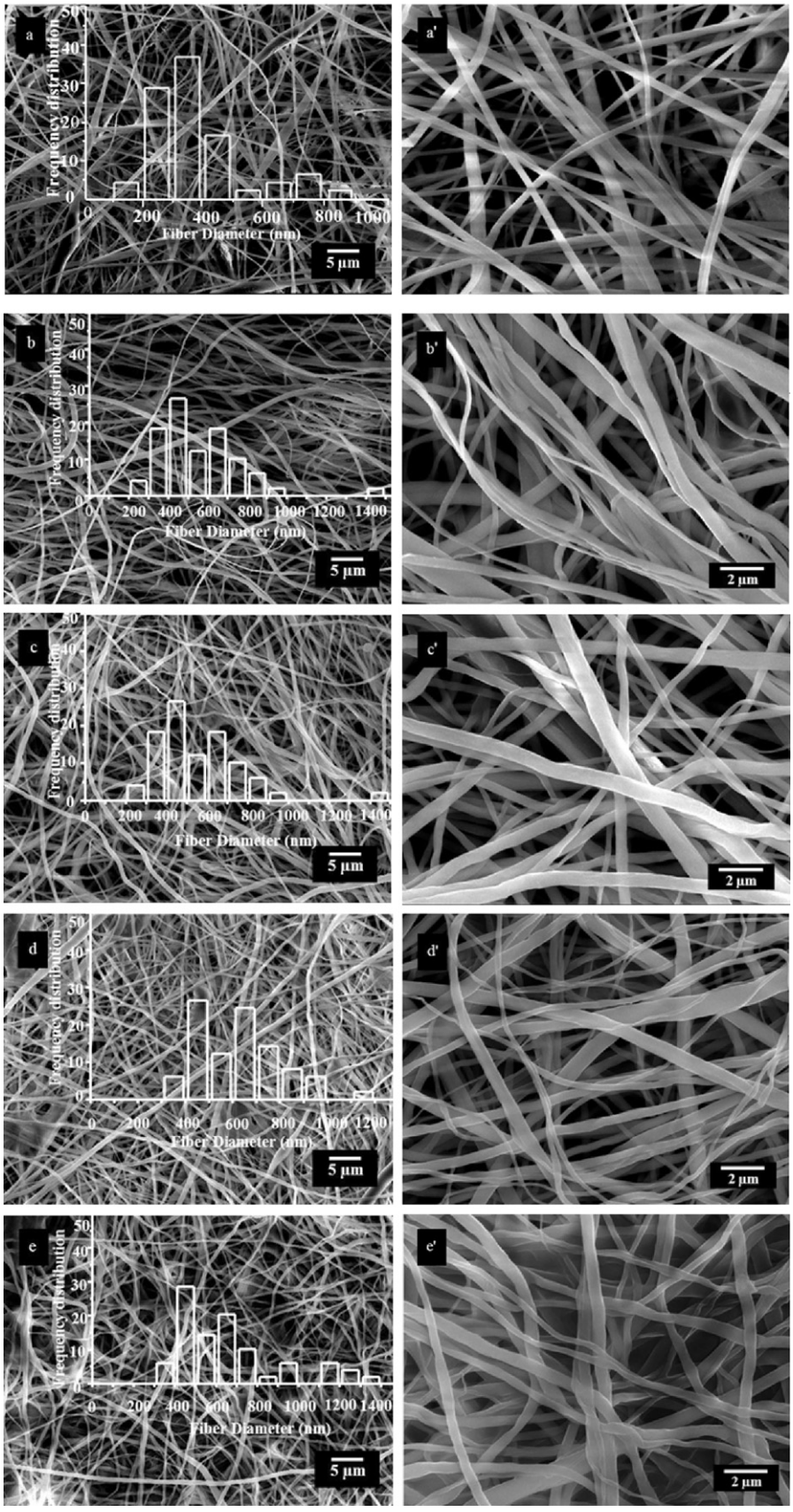

Fig. 1. FE-SEM images of (a) CA-OREC nanofibrous mats and LBL structured mats coated with: (b) $(HTCC/ALG)_5$, (c) $(HTCC/ALG)_{5.5}$, (d) $(HTCC/ALG)_{10}$ and (e) $(HTCC/ALG)_{10.5}$. The insets show the fiber size distributions. Images (a′–e′) show high magnification images of (a–e), respectively.

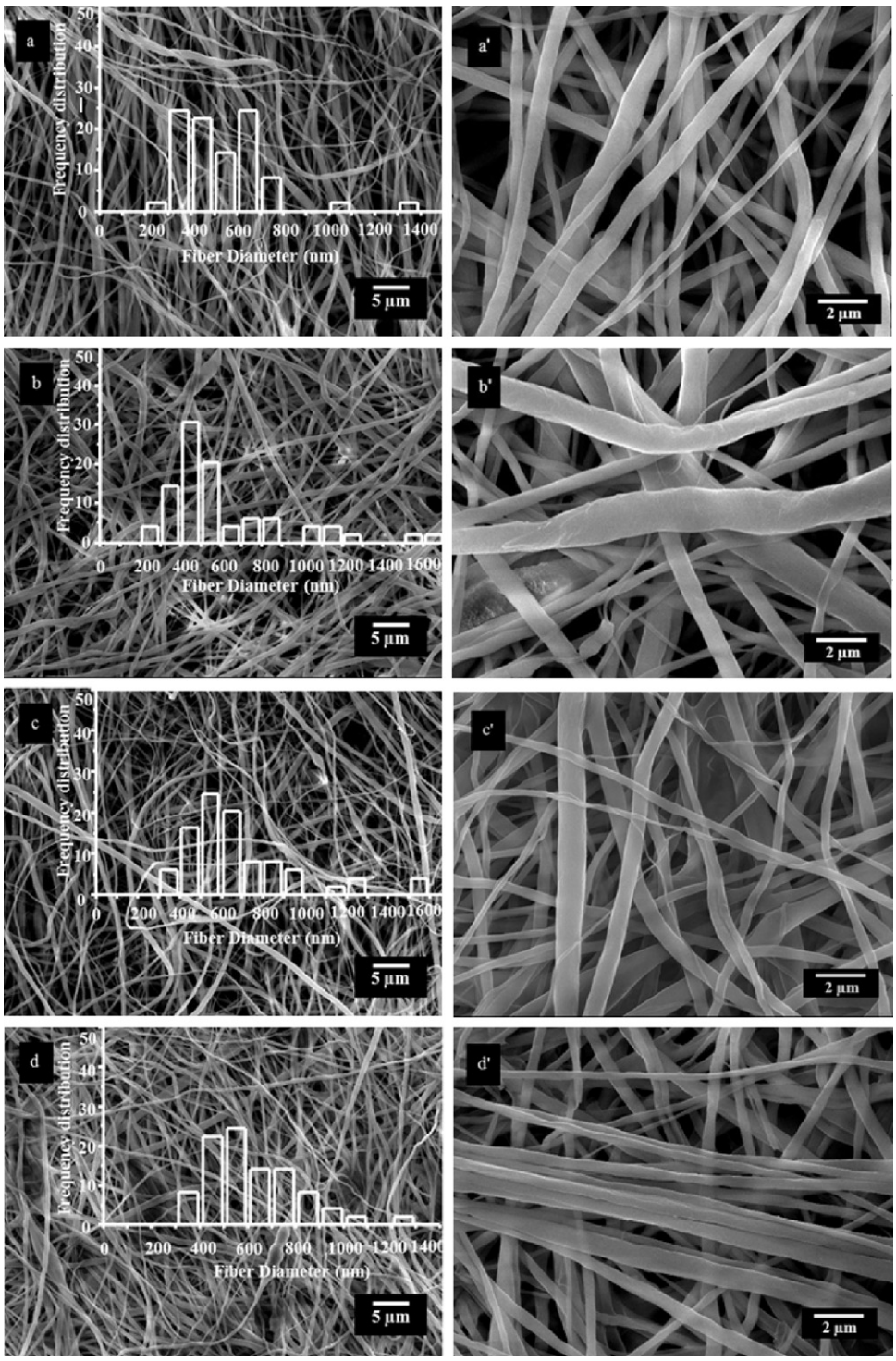

Fig. 2. FE-SEM images of LBL structured mats coated with: (a) (HTCC-OREC/ALG)$_5$, (b) (HTCC-OREC/ALG)$_{5.5}$, (c) (HTCC-OREC/ALG)$_{10}$ and (d) (HTCC-OREC/ALG)$_{10.5}$. The insets show the fiber size distributions. Images (a′–d′) show high magnification images of a–d, respectively.

air with 5% CO_2 for 24 h. The nanofibrous mats cultured with cells were then washed twice with PBS (pH 7.4) immediately after the incubation period to remove unattached L929 cells. Live/Dead assay kit (L3224, Molecular Probes Inc., USA) was added to cell-cultured samples and incubated for 30 min. Images of L929 cells on nanofibers were acquired using confocal laser scanning microscope (LSM 510 META, Zeiss, Germany). Besides, the cell morphology of L929 cells was observed from FE-SEM (Sirion 200, FEI, Holland).

2.5. MTT assay

L929 cells cultured on nanofibrous mats on the culture plate were washed gently with phosphate buffered saline (PBS) to remove untransformed solutions and unattached cells, then 25 μL MTT was added to each plate and incubated at 37 °C for 4 h. After that, DMSO (150 μL) was added to each plate to dissolve the MTT formazan purple crystals for 10 min, finally the absorbency of the solution was measured at 490 nm by using an enzyme linked

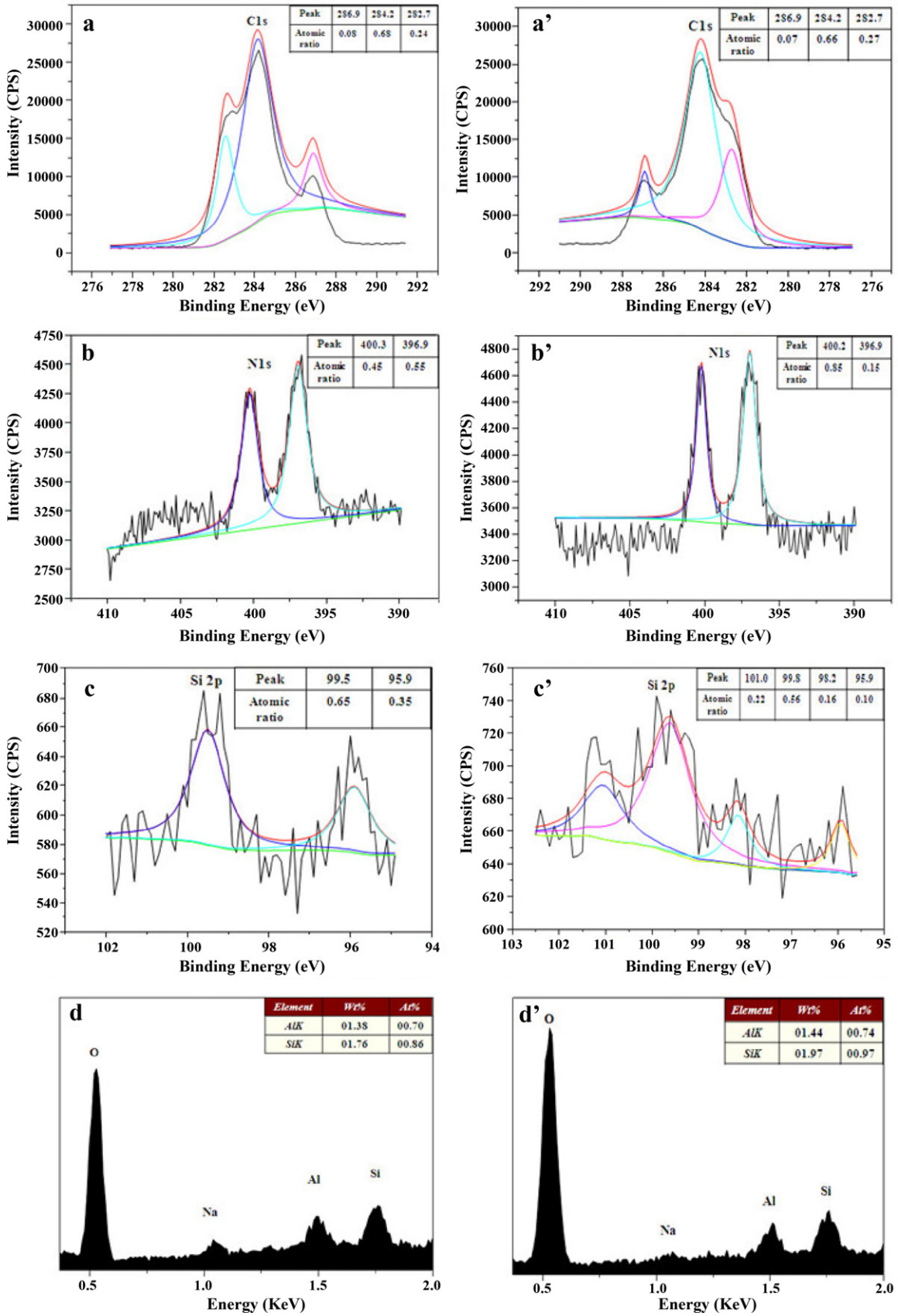

Fig. 3. XPS peak fitting curve of LBL structured nanofibrous mats coated with $(HTCC/ALG)_{10.5}$ films (a–c) and $(HTCC\text{-}OREC/ALG)_{10.5}$ films (a′–c′). EDX spectra of LBL structured nanofibrous mats coated with $(HTCC/ALG)_{10.5}$ films (d) and $(HTCC\text{-}OREC/ALG)_{10.5}$ films (d′).

Table 1
ζ-Potential of OREC, HTCC, ALG, HTCC-OREC (12:1) composites and nanofibrous mats electrospun from CA and CA-OREC.

Samples	OREC	HTCC	ALG	CA	CA-OREC	HTCC-OREC
ζ-Potential (mV)	+24	+72	−52	−28	−26	+86

immunosorbent assay (ELISA) Reader (MODEL550, Bio-Rad, USA). The results were presented as the mean ± standard deviation (SD). Significance testing was performed using one-way analysis of variance (ANOVA), followed by Bonferroni's post hoc test. Values of $^{*}p < 0.05$, $^{**}p < 0.01$ and $^{***}p < 0.001$ were considered significant.

3. Results and discussion

3.1. Morphology of electrospun and LBL structured nanofibrous mats

The influences of the number of coating bilayers and the composition of the outmost layer on the morphology and characteristic of LBL film-coated fibrous mats were investigated by FE-SEM. The morphology of the LBL structured CA-OREC mats coated with $(HTCC/ALG)_n$ films are shown in Fig. 1 and $(HTCC\text{-}OREC/ALG)_n$ films are shown in Fig. 2, respectively. The average diameter of the CA-OREC nanofibers was 376.05 ± 159.07 nm (Fig. 1a). Obviously, all the mats maintained nanofibrous 3D structure before and after LBL deposition. In Fig. 1b–e, there was no significant morphology difference between 5 and 5.5 bilayers coated mats, as well as 10 and 10.5 bilayers coated mats. However, doubling the bilayers exhibited more orderly arranged structure, much thicker average diameter and higher surface roughness by forming some irregular protuberances than those of CA-OREC fibrous mats (Deng, Wang, et al., 2011). The more bilayers used in the coating, the greater the number of protuberances that were observed. The main reason was that the different limited deposition space between adjacent fibers resulted in the imbalance of the deposition driven force and various dispersion speed of deposition materials on as-spun nanofibers (Ding, Li, Fujita, & Shiratori, 2006). Besides, several fibers with the diameter range from 1000 to 1400 nm were observed when the number of bilayers was 10.5. The above results elucidated that the number of coating bilayers was of great importance in the formation of LBL film-coated fibrous mats.

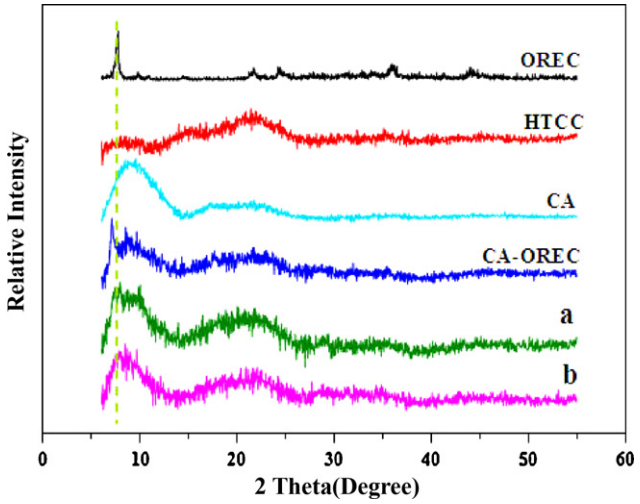

Fig. 4. XRD patterns of OREC powder, HTCC powder, CA and CA-OREC nanofibrous mats and LBL structured nanofibrous mats coated with: (a) $(HTCC/ALG)_{10.5}$ and (b) $(HTCC\text{-}OREC/ALG)_{10.5}$.

As a comparison, the FE-SEM images of LBL structured composite CA-OREC fibrous mats coated with HTCC-OREC/ALG bilayers are displayed in Fig. 2. Correspondingly, the trend in variation of fiber diameter was almost identical to that of HTCC/ALG coating. However, the fiber diameter obviously increased when OREC was added into the deposition materials. Additionally, more junctions, denser bundles and bigger protuberances formed in the resultant mats due to the higher positively charged HTCC-OREC composites (+86 mV) while the ζ-potential value of HTCC was +72 mV (Table 1). The HTCC-OREC could provide higher positive charge and larger specific area to absorb more ALG during the LBL process. Therefore, the average diameter of LBL film-coated mats containing OREC was thicker than that of HTCC-ALG films coated mats. In a word, the introduction of OREC could greatly affect the morphology of LBL films.

3.2. Composition analysis

XPS and EDX analysis were performed to investigate the surface composition of the resultant LBL structured nanofibrous mats. Fig. 3 shows the composition analysis results of the mats coated with $(HTCC/ALG)_{10.5}$ films (a–d) and $(HTCC\text{-}OREC/ALG)_{10.5}$ films (a′–d′) including XPS and EDX data, respectively. Fig. 3a and a′ detailed the spectra of the C_{1s} region in both LBL structured samples, which contained three peaks described as follows: (1) peak at 286.9 eV

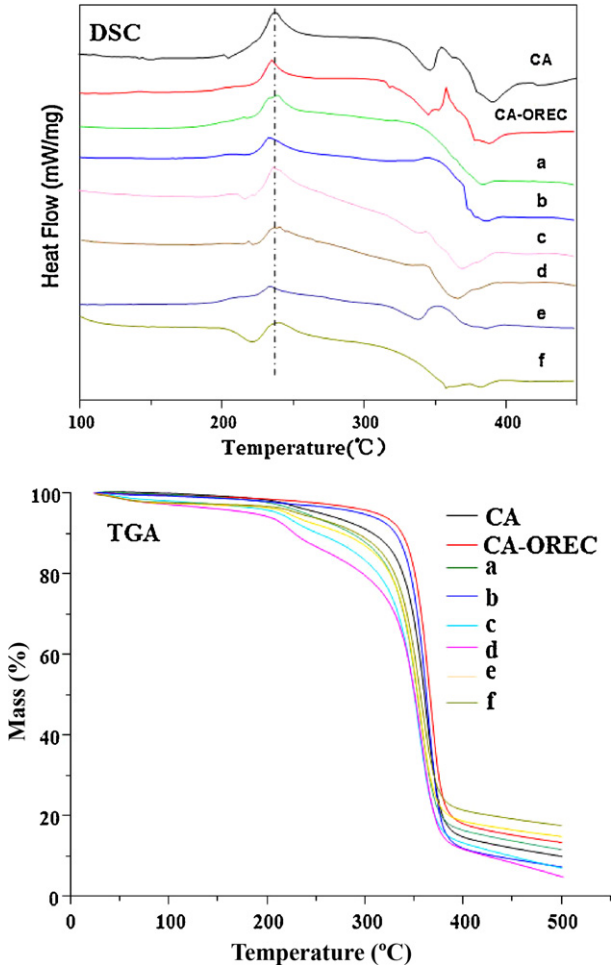

Fig. 5. DSC and TGA thermograms of CA and CA-OREC nanofibrous mats and LBL structured nanofibrous mats coated with: (a) $(HTCC/ALG)_5$, (b) $(HTCC/ALG)_{5.5}$, (c) $(HTCC/ALG)_{10}$, (d) $(HTCC/ALG)_{10.5}$, (e) $(HTCC\text{-}OREC/ALG)_{10}$ and (f) $(HTCC\text{-}OREC/ALG)_{10.5}$.

was assigned to —C—O, —C—OH and —C—OCH_3 of HTCC or ALG, and —C—N—C═O of HTCC. (2) peak around 284.2 eV was characteristic of —C—C or —C—H of HTCC or ALG and —C—NH_2 of HTCC (Ignatova et al., 2010). (3) peak at 282.6 eV was belonged to —C—Si bond formed between OREC and HTCC, ALG or CA (Račiukaitis, Brikas, Kazlauskienė, & Miškinis, 2006). Besides, the distribution ratio of each peak of LBL films coated nanofibrous mats are also displayed inset Fig. 3a and a′. The atomic ratio of —C—Si in $(HTCC/ALG)_{10.5}$ films coated nanofibrous mats was slightly lower than that of $(HTCC\text{-}OREC/ALG)_{10.5}$ coating, which demonstrated that OREC had greatly interacted with HTCC and was deposited on the CA-OREC fibrous mats successfully. In addition, XPS results gave nitrogen peaks detected on the surface of the LBL structured nanofibrous mats, which indicated that HTCC was assembled onto the CA-OREC fibers. Moreover, the N_{1s} spectrum (Fig. 3b and b′) was decomposed into two peaks centered at 396.93 eV which attributed to the assignment of the binding energy of N≡Si_3 structure and 400.26 eV which belonged to ammonium group —$N^+(CH_3)_3$ of HTCC (Deng, Wang, et al., 2011; Hua et al., 2010; Ono et al., 1999). Furthermore, the appearance of Si_{2p} peaks at 99.5 eV (—Si—Si) and 95.9 eV (silicon dioxide) verified the incorporation existed between OREC and HTCC (Fig. 3c) (Ma, Ogura, Kobayashi, & Takahashi, 2004; Pippel, Lichtenberger, & Woltersdorf, 2000). However, in Fig. 3c′ two more peaks around 101 eV (—Si—C) and 98.1 eV (low-coordinated Si) were found in $(HTCC\text{-}OREC/ALG)_{10.5}$ film-coated nanofibrous mats comparing with the Si distribution result in $(HTCC/ALG)_{10.5}$ coating (McKenna et al., 2011; Onyiriuka, Kinney, & Binkowski, 1997).

EDX spectra of $(HTCC/ALG)_{10.5}$ (Fig. 3d) and $(HTCC\text{-}OREC/ALG)_{10.5}$ films coating (Fig. 3d′) show that the contents of Si and Al are 1.97% and 1.44% in $(HTCC\text{-}OREC/ALG)_{10.5}$ films coating while that of Si and Al are 1.76% and 1.38% in $(HTCC/ALG)_{10.5}$ films coating, respectively. It was obvious that when the coating bilayers were HTCC/ALG films, Si element was only from CA-OREC template. However, when the coating bilayers were HTCC-OREC/ALG films, the content of Si increased. Herein, the increase was attributed to OREC contained LBL deposition.

Fig. 4 presents the XRD patterns of OREC powder, HTCC powder, CA nanofibrous mats, CA-OREC nanofibrous mats and resultant LBL structured nanofibrous mats. The diffraction of OREC consisted of 7.34°, 23.52°, 25.66°, 36.26° and 44.20°, and HTCC and CA appeared major crystal peaks around 21.91° and 8.67°, respectively. However, crystal peaks between 20° and 55° in CA-OREC mats and LBL films coating gradually disappeared compared to those of pure OREC. Besides, the crystalline peaks at 21.91° and 8.67° became wider and the diffraction heights of $(HTCC/ALG)_{10.5}$ films coating (Fig. 4a), $(HTCC\text{-}OREC/ALG)_{10.5}$ films coating (Fig. 4b) were gradually reduced compared to those of pure HTCC and CA. The results revealed that OREC changed the crystallinity of HTCC by the formation of the interaction structure and the restriction of molecular movement of HTCC chains (Wang et al., 2009).

The thermal stability of CA-OREC nanofibrous mats and LBL films coating is evaluated by DSC and TGA analysis (Fig. 5). Regarding to DSC analysis, it could be noted that the appearance of an exothermic event at 220 °C due to the CA crystallization (Barud et al., 2008). CA-OREC mats showed the glass transition temperature at 348.2 °C and melting temperature (T_m) at 388.3 °C, respectively. However, HTCC/ALG coating exhibited remarkable decrease in T_m and the disappearance of the glass transition, which was because of the interactions between CA-OREC mats and HTCC, and they could act as a plasticizing agent hindering glass transition and the polymer crystallization in the LBL films coating (Rodríguez, Galotto, Guarda, & Bruna, 2012). Besides, it was important to emphasize that T_g and T_m in the $(HTCC\text{-}OREC/ALG)_{10}$ and $(HTCC\text{-}OREC/ALG)_{10.5}$ films coating returned to the previous level of CA-OREC mats. The reason was that the addition of OREC could enhance the thermal stability of OREC contained LBL films coating. On the other hand, the TGA thermograms of different samples exhibited similar curves of LBL samples to that of CA-OREC mats (Fig. 5). In detail, the curves could be divided into

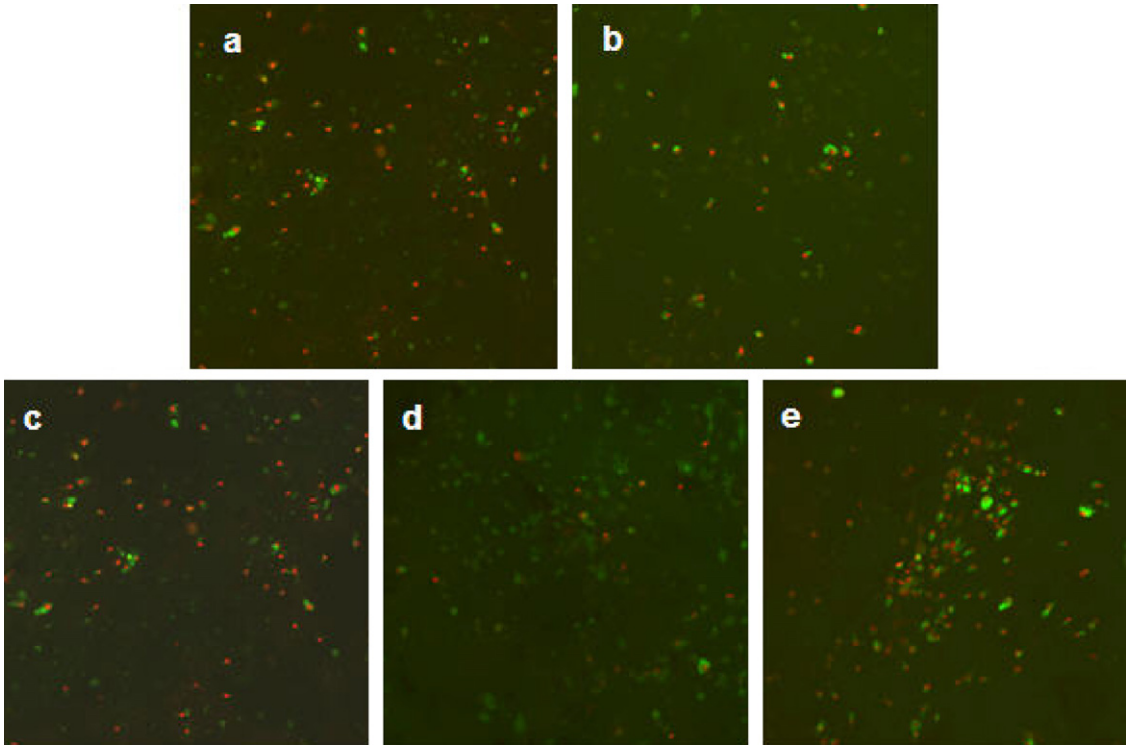

Fig. 6. Confocal microscope observation of cells cultured on (a) CA and (b) CA-OREC nanofibrous mats and LBL structured nanofibrous mats coated with: (c) $(HTCC/ALG)_5$, (d) $(HTCC/ALG)_{10.5}$ and (e) $(HTCC\text{-}OREC/ALG)_{10.5}$.

three zones: water lose, the decomposition of biopolymers and the carbonization of the degraded products to ash. The T_{max} of all LBL structured mats were slightly lower than those of CA-OREC mats. Here, T_{max} was the temperature when the rate of weight loss reached a maximum, but the mass losses of $(HTCC\text{-}OREC/ALG)_{10}$ and $(HTCC\text{-}OREC/ALG)_{10.5}$ coating were less than those of CA-OREC mats. This phenomenon stated that (HTCC-OREC/ALG) films coating exhibited better thermal stability because of the interaction between HTCC and OREC. The presence of OREC in the cellulosic structure of CA with high aspect ratio acted as barriers, which might strongly hinder the out-diffusion of the volatile decomposition products obtained from pyrolysis and prohibit the continuous decomposition of HTCC, as a direct result of the decrease in permeability (Wang et al., 2010). When HTCC chains were in a restrained state in the gallery space of the layered structure, their fractional free volume became smaller so the mobility of HTCC chains was weakened due to the interactions between HTCC molecules and OREC. Moreover, OREC containing mica layer with the high temperature resistance might contribute to the enhancement of thermal stability (Rodríguez et al., 2012; Wang et al., 2010). Furthermore, the barrier behavior was enhanced as a result of good dispersion with the increasing of the amount of OREC as barriers. Therefore, it could be concluded that the amount of OREC played an important role in improving the properties of LBL structured mats and CA-OREC template.

3.3. Cell attachment, spreading and MTT assay

Preliminary observation from the images of L929 cells is recorded by confocal microscope (Fig. 6a–e). Compared with Fig. 6a, more green spots representing live L929 cells were observed among CA-OREC nanofibrous mats in Fig. 6b because positively charged OREC was entrapped into the inner of CA fibers through electrospinning. The amount of adhesive cells on the nanofibrous mats with the outermost layer of HTCC (Fig. 6d) was much larger than that of mats with the outermost layer of ALG (Fig. 6c), because the nanofibrous mats with the outermost layer of HTCC allowed the assembly of cells into 3D structures with uniform cell

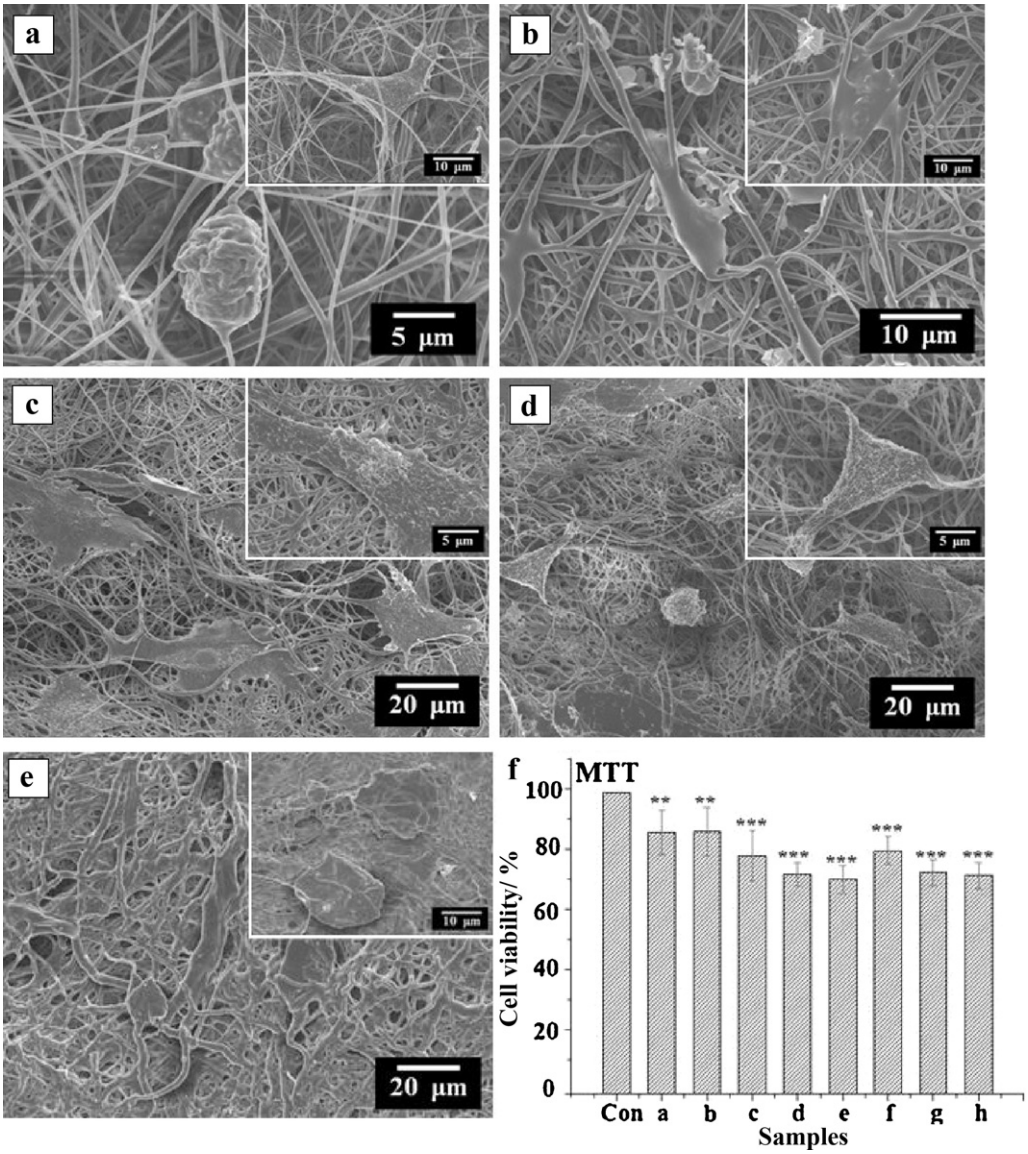

Fig. 7. FE-SEM morphology of L929 cells on (a) CA and (b) CA-OREC nanofibrous mats and LBL structured nanofibrous mats coated with: (c) $(HTCC/ALG)_5$, (d) $(HTCC/ALG)_{10.5}$ and (e) $(HTCC\text{-}OREC/ALG)_{10.5}$. Image (MTT results) shows the cell viability of untreated L929 cells (Con) and cells cultured with nanofibrous mats (a–h): (a) CA nanofibrous mats, (b) CA-OREC nanofibrous mats and LBL structured nanofibrous mats coated with: (c) $(HTCC/ALG)_5$, (d) $(HTCC/ALG)_{5.5}$, (e) $(HTCC/ALG)_{10}$, (f) $(HTCC/ALG)_{10.5}$, (g) $(HTCC\text{-}OREC/ALG)_{10}$ and (h) $(HTCC\text{-}OREC/ALG)_{10.5}$. Significant difference: $^{**}p < 0.01$, $^{***}p < 0.001$.

clusters distribution since the cationic carried HTCC could attract the cells via electrostatic interaction (Yang, Chen, & Wang, 2009). This result suggested that the outermost layer of LBL structured mats would affect the initial attachment of cells onto nanofibrous mats. Additionally, for the nanofibrous mats with the outermost layer of HTCC, the density of cells increased when the number of coating bilayers was doubled. Increasing the coating bilayers would provide a higher binding site density for cells to enhance the cell compatibility of nanofibrous mats (Bhattarai, Li, Edmondson, & Zhang, 2006; Deng et al., 2010). However, the $(HTCC\text{-}OREC/ALG)_{10.5}$ films coating (Fig. 6e) displayed less adhesive cells than that of $(HTCC/ALG)_{10.5}$ films coating which evidenced that OREC deposited on the surface of CA-OREC fibers had cytotoxic effect on L929 cells.

Fig. 7a–e shows the morphology of L929 cells cultured on the CA-OREC mats and LBL films coating. The results revealed that all the as-prepared nanofibrous mats still kept 3D microenvironment after cell culture. In Fig. 7a, cells attached to the surface of CA mats and exhibited polygonal shape with filopodia- and lamellipodia-like extensions and microvilli, and the size of the cells was from 20 to 30 μm. Fig. 7b showed numerous microvilli and discrete filopodia, and the microvilli tended to grow along the orientation of nanofibers. In Fig. 7c, it could be observed that the cells grew into the structures along the nanofibers and reached out for adjacent nanofibers in $(HTCC/ALG)_5$ films coating. In Fig. 7d, the observed cell morphology was an important indication of supported and promoted cell spreading with characteristic phenotype of filopodia- and lamellipodia-like extensions which was regarded as spreading well.

Observed from Fig. 7a–d, there was remarkable difference in morphology, which was because that the LBL structured nanofibrous mats with increased fiber diameter allowed more deposition components to be assembled, affecting the surface area to which cells could adhere, which implied that LBL films coating onto CA-OREC would be helpful in improving the cell adhesion behavior. Besides, increasing the coating bilayers would provide a higher binding site density for L929 cells to enhance the cell compatibility of mats (Deng et al., 2010). In addition, the uniform and orderly orientation of fibers obtained by LBL modification might affect the guiding of cell growth. Moreover, $(HTCC\text{-}OREC/ALG)_{10.5}$ films coating (Fig. 7e) was less functionally active than that of $(HTCC/ALG)_{10.5}$ films coating (Fig. 7d) in terms of cell attachment and spreading for L929 cells. In a previous report, it has been demonstrated that cell-scaffold interaction is dependent on the chemical characteristics of scaffolds in the first place (Zhang et al., 2005). The addition of OREC gave rise to more HTCC deposited on CA-OREC mats and a larger distance between adjacent nanofibers in $(HTCC\text{-}OREC/ALG)_{10.5}$ films coating, but too large a distance between the fibers might not allow the cells to bridge over. It could be concluded that the LBL modification of CA-OREC nanofibrous mats did have a positive effect on cell adhesion and spreading when the outmost layer was HTCC, but the addition of OREC might slightly affect cell growth.

MTT results in Fig. 7 are expressed as a percentage of the corresponding viable cells. CA mats showed slightly higher cytotoxicity than CA-OREC mats, and the cell viability of LBL films coating was identical with the results in Fig. 6, which confirmed that OREC in CA-OREC mats had little cytotoxic effect on L929 cells, but the addition of OREC into deposition films obviously affected the cytotoxicity of LBL structured mats.

4. Conclusions

LBL film-coated nanofibrous mats were successfully fabricated by electrospinning and electrostatic LBL self-assembly techniques. The EDX and XPS results evidenced that HTCC and OREC were deposited on the surface of CA-OREC template, and the addition of OREC onto LBL films resulted in thicker bilayer, larger fiber diameter and better thermal stability which could broaden their applications in food packaging, catalysis, sensors, electrochromic devices, etc. Additionally, cell attachment and MTT assay experiments suggested that both the number of coating bilayers and the composition of the outmost layer were critical points affecting the cell compatibility of the resultant scaffolds.

Acknowledgements

This project was funded by National Natural Science Foundation of China (No. 31101365). Partially supported by the Fundamental Research Funds for the Central Universities of China (No. 52902-0900202208) and the Research Funds for Innovation of College of Food Science and Technology, Huazhong Agricultural University (No. FS201102).

References

Barud, H. S., de Araújo Júnior, A. M., Santos, D. B., de Assunção, R., Meireles, C. S., Cerqueira, D. A., et al. (2008). Thermal behavior of cellulose acetate produced from homogeneous acetylation of bacterial cellulose. *Thermochimica Acta*, *471*, 61–69.

Bhattarai, N., Li, Z., Edmondson, D., & Zhang, M. (2006). Alginate-based nanofibrous scaffolds: Structural, mechanical, and biological properties. *Advanced Materials*, *18*, 1463–1467.

Boudriot, U., Dersch, R., Greiner, A., & Wendorff, J. H. (2006). Electrospinning approaches toward scaffold engineering—A brief overview. *Artificial Organs*, *30*, 785–792.

Decher, G. (1997). Fuzzy nanoassemblies: Toward layered polymeric multicomposites. *Science*, *277*, 1232–1237.

Deng, H., Li, X., Ding, B., Du, Y., Li, G., Yang, J., et al. (2011). Fabrication of polymer/layered silicate intercalated nanofibrous mats and their bacterial inhibition activity. *Carbohydrate Polymers*, *83*, 973–978.

Deng, H., Lin, P., Xin, S., Huang, R., Li, W., Du, Y., et al. (2012). Quaternized chitosan-layered silicate intercalated composites based nanofibrous mats and their antibacterial activity. *Carbohydrate Polymers*, *89*.

Deng, H., Wang, X., Liu, P., Ding, B., Du, Y., Li, G., et al. (2011). Enhanced bacterial inhibition activity of layer-by-layer structured polysaccharide film-coated cellulose nanofibrous mats via addition of layered silicate. *Carbohydrate Polymers*, *83*, 239–245.

Deng, H., Zhou, X., Wang, X., Zhang, C., Ding, B., Zhang, Q., et al. (2010). Layer-by-layer structured polysaccharides film-coated cellulose nanofibrous mats for cell culture. *Carbohydrate Polymers*, *80*, 474–479.

Ding, B., Li, C., Fujita, S., & Shiratori, S. (2006). Layer-by-layer self-assembled tubular films containing polyoxometalate on electrospun nanofibers. *Colloids and Surfaces A: Physicochemical and Engineering Aspects*, *284*, 257–262.

Du, J., & Hsieh, Y. L. (2009). Cellulose/chitosan hybrid nanofibers from electrospinning of their ester derivatives. *Cellulose*, *16*, 247–260.

European Food Safety Authority (EFSA). (2011). Scientific opinion on the safety and efficacy of bentonite (dioctahedral montmorillonite) as feed additive for all species. *EFSA Journal*, *9*, 2007–2030.

Elbakry, A., Zaky, A., Liebl, R., Rachel, R., Goepferich, A., & Breunig, M. (2009). Layer-by-layer assembled gold nanoparticles for siRNA delivery. *Nano Letters*, *9*, 2059–2064.

Giannelis, E. P. (1998). Polymer-layered silicate nanocomposites: Synthesis, properties and applications. *Applied Organometallic Chemistry*, *12*, 675–680.

Gilman, J. W. (1999). Flammability and thermal stability studies of polymer layered-silicate (clay) nanocomposites. *Applied Clay Science*, *15*, 31–49.

Hartgerink, J. D., Beniash, E., & Stupp, S. I. (2001). Self-assembly and mineralization of peptide-amphiphile nanofibers. *Science*, *294*, 1684–1688.

Hua, M. Y., Yang, H. W., Chuang, C. K., Tsai, R. Y., Chen, W. J., Chuang, K. L., et al. (2010). Magnetic-nanoparticle-modified paclitaxel for targeted therapy for prostate cancer. *Biomaterials*, *31*, 7355–7363.

Huang, Z. M., Zhang, Y. Z., Kotaki, M., & Ramakrishna, S. (2003). A review on polymer nanofibers by electrospinning and their applications in nanocomposites. *Composites Science and Technology*, *63*, 2223–2253.

Ignatova, M. G., Manolova, N. E., Toshkova, R. A., Rashkov, I. B., Gardeva, E. G., Yossifova, L. S., et al. (2010). Electrospun nanofibrous mats containing quaternized chitosan and polylactide with in vitro antitumor activity against HeLa cells. *Biomacromolecules*, *11*, 1633–1645.

Kanani, A. G., & Bahrami, S. H. (2010). Review on electrospun nanofibers scaffold and biomedical applications. *Trends in Biomaterials and Artificial Organs*, *24*, 930115.

Ma, W., Ogura, M., Kobayashi, T., & Takahashi, H. (2004). Preparation of solar grade silicon from optical fibers wastes with thermal plasmas. *Solar Energy Materials and Solar Cells*, *81*, 477–483.

McKenna, J., Patel, J., Mitra, S., Soin, N., Švrček, V., Maguire, P., et al. (2011). Synthesis and surface engineering of nanomaterials by atmospheric-pressure microplasmas. *European Physical Journal-Applied Physics*, *56*, 323001.

Ono, H., Ikarashi, T., Miura, Y., Hasegawa, E., Ando, K., & Kitano, T. (1999). Bonding configurations of nitrogen absorption peak at 960 cm in silicon oxynitride films. *Applied Physics Letters*, *74*, 203.

Onyiriuka, E. C., Kinney, L. D., & Binkowski, N. J. (1997). Adhesion and delamination of tantalum and chromium films on glass. *Journal of Adhesion Science and Technology*, *11*, 929–940.

Pippel, E., Lichtenberger, O., & Woltersdorf, J. (2000). Identification of silicon oxycarbide bonding in Si–CO-glasses by EELS. *Journal of Materials Science Letters*, *19*, 2059–2060.

Qin, C., Xiao, Q., Li, H., Fang, M., Liu, Y., Chen, X., et al. (2004). Calorimetric studies of the action of chitosan-N-2-hydroxypropyl trimethyl ammonium chloride on the growth of microorganisms. *International Journal of Biological Macromolecules*, *34*, 121–126.

Račiukaitis, G., Brikas, M., Kazlauskienė, V., & Miškinis, J. (2006). Doping of silicon with carbon during laser ablation process. *Applied Physics A: Materials Science & Processing*, *85*, 445–450.

Reneker, D. H., & Chun, I. (1996). Nanometre diameter fibres of polymer, produced by electrospinning. *Nanotechnology*, *7*, 216.

Rodríguez, F. J., Galotto, M. J., Guarda, A., & Bruna, J. E. (2012). Modification of cellulose acetate films using nanofillers based on organoclays. *Journal of Food Engineering*, *110*, 262.

Sinha Ray, S., & Bousmina, M. (2005). Biodegradable polymers and their layered silicate nanocomposites: In greening the 21st century materials world. *Progress in Materials Science*, *50*, 962–1079.

Venugopal, J., Low, S., Choon, A. T., & Ramakrishna, S. (2008). Interaction of cells and nanofiber scaffolds in tissue engineering. *Journal of Biomedical Materials Research Part B: Applied Biomaterials*, *84*, 34–48.

Wang, X., Du, Y., Luo, J., Yang, J., Wang, W., & Kennedy, J. F. (2009). A novel biopolymer/rectorite nanocomposite with antimicrobial activity. *Carbohydrate Polymers*, *77*, 449–456.

Wang, X., Du, Y., Yang, J., Wang, X., Shi, X., & Hu, Y. (2006). Preparation, characterization and antimicrobial activity of chitosan/layered silicate nanocomposites. *Polymer*, *47*, 6738–6744.

Wang, X., Liu, B., Ren, J., Liu, C., Wang, X., Wu, J., et al. (2010). Preparation and characterization of new quaternized carboxymethyl chitosan/rectorite nanocomposite. *Composites Science and Technology*, *70*, 1161–1167.

Xiao, S., Wu, S., Shen, M., Guo, R., Huang, Q., Wang, S., et al. (2009). Polyelectrolyte multilayer-assisted immobilization of zero-valent iron nanoparticles onto polymer nanofibers for potential environmental applications. *ACS Applied Materials & Interfaces*, *1*, 2848–2855.

Xu, R., Feng, X., Li, W., Xin, S., Wang, X., Deng, H., et al. (2012). Novel polymer-layered silicate intercalated composite beads for drug delivery. *Journal of Biomaterials Science, Polymer Edition*, http://dx.doi.org/10.1163/156856211X619630

Yang, X., Chen, X., & Wang, H. (2009). Acceleration of osteogenic differentiation of preosteoblastic cells by chitosan containing nanofibrous scaffolds. *Biomacromolecules*, *10*, 2772–2778.

Zhang, Y., Venugopal, J., Huang, Z. M., Lim, C., & Ramakrishna, S. (2005). Characterization of the surface biocompatibility of the electrospun PCL-collagen nanofibers using fibroblasts. *Biomacromolecules*, *6*, 2583–2589.